The Astrophysical Journal, 939:106 (17pp), 2022 November 10 https://doi.org/10.3847/1538-4357/ac972b

A Short Gamma-Ray Burst from a Protomagnetar Remnant

N. Jordana-Mitjans[1], C. G. Mundell[1], C. Guidorzi[2,3,4], R. J. Smith[5], E. Ramírez-Ruiz[6,7], B. D. Metzger[8,9], S. Kobayashi[5], A. Gomboc[10], I. A. Steele[5], M. Shrestha[5], M. Marongiu[11], A. Rossi[12], and B. Rothberg[13,14]
[1] Department of Physics, University of Bath, Claverton Down, Bath, BA2 7AY, UK; N.Jordana@bath.ac.uk
[2] Department of Physics and Earth Science, University of Ferrara, via Saragat 1, I-44122, Ferrara, Italy
[3] INFN—Sezione di Ferrara, Via Saragat 1, I-44122 Ferrara, Italy
[4] INAF—Osservatorio di Astrofisica e Scienza dello Spazio di Bologna, Via Piero Gobetti 101, I-40129 Bologna, Italy
[5] Astrophysics Research Institute, Liverpool John Moores University, 146 Brownlow Hill, Liverpool, L3 5RF, UK
[6] Department of Astronomy and Astrophysics, University of California, Santa Cruz, CA 95064, USA
[7] DARK, Niels Bohr Institute, University of Copenhagen, Jagtvej 128, DK-2200, Copenhagen, Denmark
[8] Columbia Astrophysics Laboratory, Columbia University, New York, NY 10027, USA
[9] Center for Computational Astrophysics, Flatiron Institute, New York, NY 10010, USA
[10] Center for Astrophysics and Cosmology, University of Nova Gorica, Vipavska 13, 5000 Nova Gorica, Slovenia
[11] INAF—Osservatorio Astronomico di Cagliari, via della Scienza, 5-I-09047 Selargius, Italy
[12] INAF—Osservatorio di Astrofisica e Scienza dello Spazio, via Piero Gobetti 93/3, I-40129 Bologna, Italy
[13] LBT Observatory, University of Arizona, 933 N.Cherry Avenue,Tucson, AZ 85721, USA
[14] George Mason University, Department of Physics & Astronomy, MS 3F3, 4400 University Drive, Fairfax, VA 22030, USA
Received 2022 July 5; revised 2022 August 26; accepted 2022 September 22; published 2022 November 10

Abstract

The contemporaneous detection of gravitational waves and gamma rays from GW170817/GRB 170817A, followed by kilonova emission a day after, confirmed compact binary neutron star mergers as progenitors of short-duration gamma-ray bursts (GRBs) and cosmic sources of heavy *r*-process nuclei. However, the nature (and life span) of the merger remnant and the energy reservoir powering these bright gamma-ray flashes remains debated, while the first minutes after the merger are unexplored at optical wavelengths. Here, we report the earliest discovery of bright thermal optical emission associated with short GRB 180618A with extended gamma-ray emission—with ultraviolet and optical multicolor observations starting as soon as 1.4 minutes post-burst. The spectrum is consistent with a fast-fading afterglow and emerging thermal optical emission 15 minutes post-burst, which fades abruptly and chromatically (flux density $F_\nu \propto t^{-\alpha}$, $\alpha = 4.6 \pm 0.3$) just 35 minutes after the GRB. Our observations from gamma rays to optical wavelengths are consistent with a hot nebula expanding at relativistic speeds, powered by the plasma winds from a newborn, rapidly spinning and highly magnetized neutron star (i.e., a millisecond magnetar), whose rotational energy is released at a rate $L_{\rm th} \propto t^{-(2.22\pm0.14)}$ to reheat the unbound merger-remnant material. These results suggest that such neutron stars can survive the collapse to a black hole on timescales much larger than a few hundred milliseconds after the merger and power the GRB itself through accretion. Bright thermal optical counterparts to binary merger gravitational wave sources may be common in future wide-field fast-cadence sky surveys.

Unified Astronomy Thesaurus concepts: High energy astrophysics (739); Time domain astronomy (2109); Gamma-ray bursts (629); Magnetars (992); Polarimetry (1278)

Supporting material: machine-readable table

1. Introduction

Gamma-ray bursts (GRBs) are bright extragalactic flashes of gamma-ray radiation and briefly the most energetic explosions in the universe (Gehrels et al. 2009). Their catastrophic origin —the merger of compact star binaries for short-duration GRBs (Paczynski 1986; Fryer et al. 1999; Lee & Ramirez-Ruiz 2007; Tanvir et al. 2013; Abbott et al. 2017b) or the collapse of massive stars for long GRBs (Woosley 1993; Bloom et al. 1999; MacFadyen & Woosley 1999)— drives the formation of a newborn compact remnant (black hole or magnetar) that powers two highly relativistic jets. In the framework of the standard fireball model and after the initial prompt gamma-ray emission (e.g., Mészáros & Rees 1997; Piran 1999), the relativistic ejecta are decelerated by the circumburst medium by a pair of external shocks: a short-lived reverse shock and a forward shock (e.g., Rees & Meszaros 1992; Sari & Piran 1999; Kobayashi 2000). This lagging emission called the afterglow radiates via synchrotron emission and can be detected seconds to years after the burst at wavelengths across the electromagnetic spectrum (e.g., Costa et al. 1997; van Paradijs et al. 1997; Gehrels et al. 2009).

Short GRBs represent 9% of the total detected by the Swift Burst Alert Telescope (BAT; Lien et al. 2016), resulting in a significantly lower frequency of real-time multiwavelength studies when compared to long GRBs. Additionally, the optical counterparts of short GRBs are typically a few hundred times fainter than those of massive star collapse origin (Kann et al. 2011). This challenges the early follow-up and the study of short GRBs with small and medium-sized telescopes, and limits the available data to several hours post-burst, in the kilonovae time domain (Tanvir et al. 2013; Abbott et al. 2017a; Troja et al. 2018).

Successful broadband follow-up of short GRBs began with the discovery of the X-ray and optical afterglow of GRB

050709 (Fox et al. 2005; Hjorth et al. 2005; Villasenor et al. 2005), and first radio afterglow of GRB 050724 (Berger et al. 2005). After these events, there have been numerous detections of short GRB afterglows (e.g., Fong et al. 2015), including the first detection of a kilonova (Berger et al. 2013; Tanvir et al. 2013) and the joint discovery of the GW170817/GRB 170817A/kilonova, which confirmed that binary neutron stars are progenitors of at least some short GRBs (Abbott et al. 2017a, 2017b; Goldstein et al. 2017; Tanvir et al. 2017). Still, the remnant of neutron star binary mergers remains largely debated (Murguia-Berthier et al. 2014, 2021; Ruiz & Shapiro 2017; Metzger et al. 2018; Margalit & Metzger 2019; Metzger 2019; Beznogov et al. 2020; Mösta et al. 2020). More recently, giant flares from extragalactic magnetars have been associated as sources of low-luminosity short-duration GRBs (Fermi-LAT Collaboration et al. 2021; Roberts et al. 2021; Svinkin et al. 2021).

Here, we present the early-time multiwavelength observations and polarization constraint of GRB 180618A, a short GRB with extended emission (e.g., Norris & Bonnell 2006). So far, the only polarization measurement of a short GRB optical counterpart has been the $P = 0.50\% \pm 0.07\%$ detection in the GW170817 kilonova at $\approx$1.5 days after the merger (Covino et al. 2017)—consistent with polarization from Galactic dust. Short GRBs with extended soft gamma-ray emission are rarely studied at lower frequencies (Perley et al. 2009; Knust et al. 2017), as they are a small fraction of the total detected by the BAT ($\approx$1%; Lien et al. 2016). Such elusive objects are merger candidates and display the typical short hard prompt gamma-ray emission followed by variable soft gamma-ray emission spanning 10−100 s (Norris & Bonnell 2006; Perley et al. 2009; Hu et al. 2014; Kaneko et al. 2015). Candidate mechanisms powering such extended gamma-ray emission after the merger include late-time activity from the central engine (Metzger et al. 2008; Bucciantini et al. 2012), interaction with a pulsar-wind cavity (Ramirez-Ruiz et al. 2019), prolonged accretion from the gravitationally bound material ejected premerger (Lee & Ramirez-Ruiz 2007; Rosswog 2007; Lee et al. 2009), or a two-component outflow viewed slightly off-axis (Barkov & Pozanenko 2011).

This work is structured as follows. In Section 2, we present the GRB 180618A optical observations and data reduction of the UltraViolet and Optical Telescope (UVOT) and the 2 m Liverpool Telescope (LT)—including the RINGO3 multi-wavelength polarimeter/imager and the IO:O camera. In addition, we detail the 8.4 m Large Binocular Telescope (LBT) observations; that is, deep-field imaging with the Large Binocular Cameras (LBC) and spectroscopy of the host galaxy candidates with the Multi-Object Double Spectrographs (MODS). In Section 3, the properties of the optical and gamma-ray emission are presented. In Section 4, the physical origin of the peculiar multiwavelength emission of GRB 180618A is discussed—in particular, the optical emission. In Section 5, the implications of the GRB 180618A results are discussed in the wide context of neutron star mergers. In Section 6, we summarize our findings.

We assume a flat ΛCDM cosmology with $\Omega_m = 0.32$, $\Omega_\Lambda = 0.68$, and $h = 0.67$, as reported by Planck Collaboration et al. (2020). We adopt the convention $F_\nu \propto t^{-\alpha}\nu^{-\beta}$, where α is the temporal index, and β is the spectral index. Note that the spectral index is related to the photon index like $\beta = \beta_{\rm PI} - 1$.

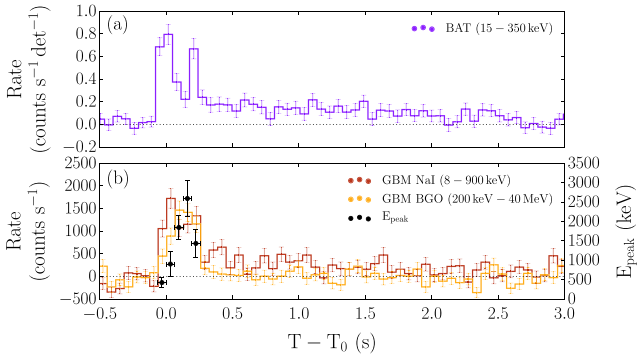

Figure 1. GRB 180618A light curves at 64 ms resolution as detected by the BAT and the GBM instruments. (a) Count rate per enabled detector of the 15−350 keV energy band of the BAT. (b) Count rates of the 8−900 keV energy band of the GBM sodium iodide (NaI) detector, and the 200 keV −40 MeV of the GBM bismuth germanate (BGO) detector. In a different y-axis, we present the evolution of the peak energy ($E_{\rm peak}$); the values were derived from a cutoff power-law model fit to the 8 keV−40 MeV νF_ν spectrum. In the x-axis, T_0 corresponds to the BAT trigger time.

Unless stated otherwise, all uncertainties reported in this paper are given at the 1σ confidence level.

2. Observations and Data Reduction

On 2018 June 18 at $T_0 = 00{:}43{:}13$ universal time (UT), the BAT from the Neil Gehrels Swift Observatory triggered an alert for GRB 180618A (Meegan et al. 2009; LaPorte et al. 2018). GRB 180618A was detected by the BAT (Barthelmy et al. 2005; Sakamoto et al. 2018), the Gamma-ray Burst Monitor (GBM; Meegan et al. 2009; Hamburg et al. 2018), and the Konus instrument from the Wind satellite (Aptekar et al. 1995; Svinkin et al. 2018) as a short-duration and spectrally hard bright GRB with a long-duration weak emission tail at low gamma-ray energies (see Figure 1). Further GRB 180618A detections include the Astrosat Cadmium Zinc Telluride Imager (CZTI; Singh et al. 2014; Sharma et al. 2018) and the Insight Hard X-ray Modulation Telescope (HXMT; Liu et al. 2020; Song et al. 2022).

2.1. Ultraviolet and Optical Light Curves

At 86 s after the detection of GRB 180618A by the BAT, the UVOT (Roming et al. 2005) from the Neil Gehrels Swift Observatory started optical observations in an unfiltered band (*white*). Subsequently, the UVOT continued observations with the *uvw1, uvm2, uvw2* ultraviolet and the *v, b, u* optical filters (see Figure 2). At 202.5 s after the BAT alert, the 2 m fully robotic LT (Steele 2004)—with site at Roque de Los Muchachos Observatory (ORM; Spain)— automatically started follow-up observations (Guidorzi et al. 2006) with the RINGO3 three-band polarimeter and imager (Arnold et al. 2012). The LT observations consisted of three consecutive observing sequences of 10 minutes each with RINGO3 in three simultaneous bands (*BV, R, I*), followed by six single 10 s exposures with the *r* filter of the IO:O optical wide-field camera[15] and two extra observation sets of 10 minutes with RINGO3. Three 300 s exposures with the IO:O *g, r, i* filters were also scheduled via the LT *phase2UI*[16] and autonomously executed by the LT 7.4×10^4 s post-burst.

[15] https://telescope.livjm.ac.uk/TelInst/Inst/IOO/
[16] https://telescope.livjm.ac.uk/PropInst/Phase2/

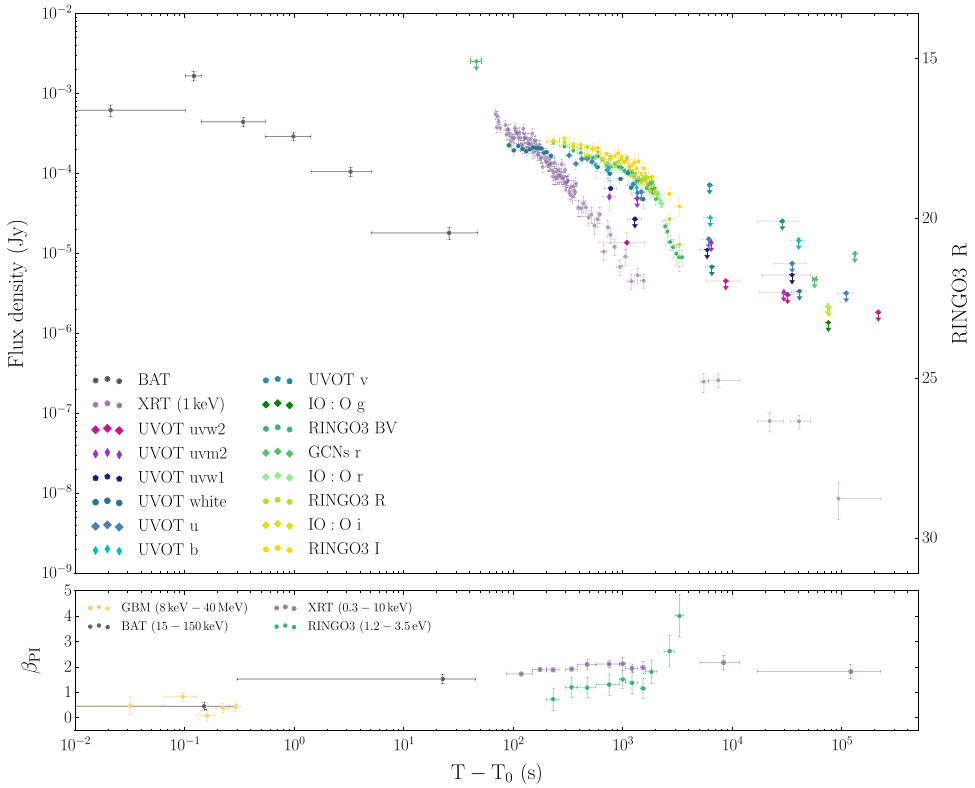

Figure 2. GRB 180618A light curves at the gamma-ray, X-ray, ultraviolet and optical bands. The data correspond to the Swift BAT, Swift XRT, Swift UVOT *white, v, b, u, uvw1, uvm2, uvw2* bands; LT RINGO3 *BV, R, I* bands; and LT IO:O *g, r, i* bands. The Swift BAT and XRT observations were obtained from the web interface provided by the Leicester University (Evans et al. 2009); the BAT data were binned to a signal-to-noise ratio of 7, and the absorbed 0.3−10 keV XRT light curve was converted to the observed flux density at 1 keV. For completeness, we include the optical observations and upper limits reported in the Gamma-ray Coordination Network (GCN) from the MASTER II (Tyurina et al. 2018), Tien Shan Astronomical Observatory (Mazaeva et al. 2018), and Xinglong-2.16 m (Zhu et al. 2018). Note that the GCN observations do not include filter corrections. In the *x*-axis, T_0 corresponds to the BAT trigger time. In the *y*-axis, the flux density is converted to the RINGO3 *R* magnitude. Detections have 1σ error bars, and nondetections are presented as 3σ upper limits—note that the MASTER data have 5σ upper limits. In the bottom panel, we present the temporal evolution of the photon index in the GBM 8 keV−40 MeV gamma-ray band, the BAT 15−150 keV gamma-ray band, the XRT 0.3−10 keV X-ray band, and the RINGO3 1.2−3.5 eV optical band.

The UVOT photometry (Vega; see Table 1) was derived from Level 1/2 products, which are already preprocessed by the telescope pipeline. We used the Level 1 event products to get a higher temporal resolution. They were converted into sky-coordinated data with the *coordinator* tool from the *HEASoft* v6.22.1 package (Blackburn 1995), and the hot pixels were removed with *uvotscreen*. The photometry was background-subtracted and measured with *uvotevtlc* using the default aperture radius of 5″ from the instrument calibration (Poole et al. 2008; Breeveld et al. 2011). For the Level 2 images, we used the equivalent *uvotsource* tool. Furthermore, the images were aligned with *uvotskycorr* and co-added with *uvotisum*, requiring a minimum significance of 3σ for the detection of the optical transient. The stacked frames in which the optical transient did not reach the signal-to-noise ratio threshold are reported as 3σ flux upper limits in Table 1.

RINGO3 photometry (Vega; see Table 1) was derived by integrating the source photon counts across the eight polaroid positions (e.g., Jordana-Mitjans et al. 2020)—thus canceling any polarization signal. Each 10 minutes of integration consist of 10 single 1 minute exposures (see Figure 3), from which we individually derived the photometry using the *Astropy Photutils* package (Bradley et al. 2016). If the signal-to-noise ratio did not reach a minimum 3σ significance, we co-added consecutive frames. The RINGO3 magnitudes and flux density were absolute-calibrated in the Vega system following a standard procedure (see, e.g., Jordana-Mitjans et al. 2020) with observations of five dereddened A0-type stars (BD +30 2355, BD +67 675, BD +25 2478, HD 96781, HD 208368; Høg et al. 2000). The standard stars and the GRB 180618A

Table 1
GRB 180618A Ultraviolet and Optical Photometry Corresponding to the Swift UVOT *white, v, b, u, uvw1, uvm2, uvw2* Bands; LT RINGO3 *BV, R, I* Bands; and LT IO:O *g, r, i* Bands

Band	$t_{mid} - T_0$ (s)	$t_{exp}/2$ (s)	mag	mag $_{err}$	F_ν (Jy)	$F_{\nu\,err}$ (Jy)
white	91	5	17.32	0.13	2.27e-04	2.7e-05
white	101	5	17.48	0.14	1.96e-04	2.6e-05
white	111	5	17.34	0.13	2.23e-04	2.6e-05
white	121	5	17.44	0.13	2.04e-04	2.5e-05
white	131	5	17.51	0.14	1.91e-04	2.5e-05
white	141	5	17.45	0.13	2.02e-04	2.5e-05
white	151	5	17.39	0.13	2.13e-04	2.5e-05
white	161	5	17.40	0.13	2.11e-04	2.5e-05
white	…	…	…	…	…	…

Note. t_{mid} corresponds to the mean observing time, T_0 is the BAT trigger time, and t_{exp} is the length of the observing time window. Note that the photometry is not corrected for neither Galactic, i.e., with reddening $E(B-V)_{MW} = 0.065 \pm 0.003$ (Schlegel et al. 1998), nor host galaxy extinction. Table 1 is published in its entirety in machine-readable format. A portion is shown here for guidance regarding its form and content.

(This table is available in its entirety in machine-readable form.)

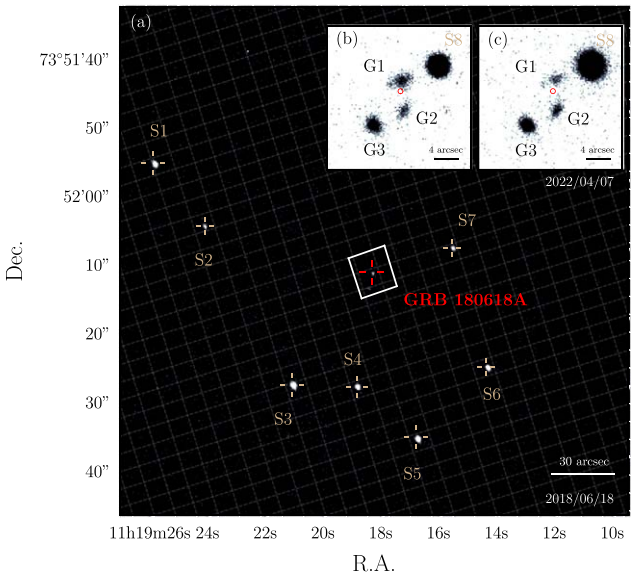

Figure 3. Observing fields of the GRB 180618A sky region. The GRB 180618A location is labeled in red, the stars (S) in light brown, and the galaxies (G) in black. (a) The 2 m LT *I*-band RINGO3 image of the GRB 180618A optical transient. (b) The *r*-band LBC image from the 8.4 m LBT. (c) The LBT *z*-band image. The field of view of the magnified LBT images corresponds to the white rectangle of panel (a). The LBT images reveal three galaxies at a similar redshift near the UVOT subarcsec localization of GRB 180618A (shown in red at the 90% confidence level). The G1 is the host galaxy of short GRB 180618A, with spectroscopic redshift $z = 0.554 \pm 0.001$.

field observations were scheduled via the LT *phase2UI* using the same instrumental setup of the night of the burst, and they were executed on 2019 June 13 and 16. This spectral calibration added a ≈0.07 mag uncertainty to the photometry. To test the instrument stability during observations, we checked the flux variability of five stars in the GRB 180618A field of view (see Figure 4). Using the temporal binning of the GRB 180618A light curves, the stars displayed on average a ≈0.04 mag deviation from the mean.

The IO:O camera photometry (AB; see Table 1) was derived for each of the 10 s individual frames. For the observing sequence 7.4×10^4 s post-burst, we integrated the observations into a single 900 s exposure per band. The optical transient was not detected, and the flux upper limits are presented in Table 1 at the 3σ confidence level. We calibrated the IO:O bands by crossmatching 10 12−17 mag stars from the Sloan Digital Sky Survey (SDSS) Data Release 12 catalog (Alam et al. 2015).

2.2. Optical Polarimetry

In the RINGO3 configuration, we measure the polarization of a source by extracting the flux at each of the eight polaroid positions (e.g., Jordana-Mitjans et al. 2020), which we then convert to Stokes parameters $(q - u)$ following Clarke & Neumayer (2002). The polarization uncertainties are derived from a Monte Carlo error propagation, starting from 10^6 flux values.

We measured the instrumental $q - u$ using ≈75 measurements of seven unpolarized standards per band (BD +32 3739, BD +33 2642, BD +28 4211, HD 212311, HD 14069, HD 109055, G191B2B; Turnshek et al. 1990; Schmidt et al. 1992), which were observed during 200 days before and 10 days after the date of the burst. Note that we used an asymmetric time window of data given a small shift of $\Delta u \approx 0.005$ in the instrumental u parameter 10 days post-burst. For the chosen time window, there was no significant drift of the instrumental $q - u$, and the Pearson's correlation coefficients were low $|r| < 0.1$ with p-values > 0.3.

To derive the most constraining polarization measurement for GRB 180618A, we used the entire 10 minutes epoch corresponding to $t_1 = 203$–800 s post-burst of the *BV* band, which is the RINGO3 band with the highest signal-to-noise ratio. We detected the optical transient at a signal-to-noise ratio of ≈27 in each of the eight images of the polaroid. At this signal-to-noise ratio level, the observed polarization ($P \approx 1\%$) was within the instrument sensitivity, and we estimate a 2σ upper limit of $P_{BV} < 6.1\%$. Due to the slowly fading emission during the second and third observing epochs, $t_2 = 822$–1417 s and $t_3 = 1438$–2035 s post-burst, respectively, the polarization upper limits could still be derived but were less well constrained, with $P_{BV,\{t_2,t_3\}} < 10.7\%, 17.0\%$ (2σ). For the *R* and *I* bands, the 2σ upper limits for the three epochs are $P_{R,\{t_1,t_2,t_3\}} < 14.5\%, 30.2\%, 37.0\%$ and $P_{I,\{t_1,t_2,t_3\}} < 23.5\%, 36.8\%, 38.6\%$. We note that the RINGO3 depolarization factor (Jordana-Mitjans et al. 2021) is negligible in the *BV* band ($D_{BV} = 1$) and small in the *R* and *I* bands ($D_{\{R,I\}} = 0.98, 0.94$).

2.3. LBT Photometry

To search for the GRB 180618A host galaxy, and thus determine the GRB 180618A redshift, we used the LBT (Hill et al. 2006)—an optical/infrared telescope with twin 8.4 m mirrors located on the Mt. Graham International Observatory, Arizona, USA.

On 5 April 2022, deep-field *r*- and *z*-band imaging of the GRB 180618A location were acquired with the LBC (Ragazzoni et al. 2000; Giallongo et al. 2008). The total exposure time for each filter was 36 minutes, and the data were reduced with the data reduction pipeline developed by the Istituto Nazionale di Astrofisica (INAF-Osservatorio Astronomico di Roma; Fontana et al. 2014), which includes bias subtraction and flat-fielding, bad-pixel and cosmic-ray masking, astrometric calibration, and co-addition. The average seeing was ≈1.″4, and the mean airmass of the observations was ≈1.4. The LBC photometry (AB) achieved limiting magnitudes of $r_{\rm lim} = 26.3$ mag and $z_{\rm lim} = 25.6$ mag (3σ limits). In both images, we found three galaxies (G1, G2, and G3; see Figure 3) at a projected angular distance of $d_{\rm G1} = 1.''6$, $d_{\rm G2} = 3.''7$, and $d_{\rm G3} = 7.''7$ from the UVOT subarcsec localization of GRB 180618A (Siegel et al. 2018). The G3 galaxy was already cataloged by the SDSS (Alam et al. 2015), with a photometric redshift of $z_{\rm G3} = 0.54 \pm 0.03$, and brightness $r_{\rm band,G3} = 22.4 \pm 0.3$ mag and $z_{\rm band,G3} = 21.2 \pm 0.6$ mag. The G1 and G2 galaxies were uncatalogued in the SDSS but identified in the O'Connor et al. (2022) and Fong et al. (2022) surveys of short GRBs host galaxies. From the LBC images, we measured $r_{\rm band,G1} = 22.98 \pm 0.06$ mag, $r_{\rm band,G2} = 23.58 \pm 0.11$ mag in the *r* band, and $z_{\rm band,G1} = 22.62 \pm 0.10$ mag, $z_{\rm band,G2} = 22.48 \pm 0.09$ mag in the *z* band.

2.4. LBT Spectroscopy

On 2022 April 8, optical spectroscopy of the G1 and G2 galaxies was obtained with the MODS (Pogge et al. 2010), i.e., MODS-1 and MODS-2. Each MODS contains a red and blue channel for spectroscopy. Both MODS were configured to use the dual grating mode (0.32 μm–1.05 μm coverage) and a 1.″2 wide slit ($R \approx 630$–1350 resolution). A position angle of 179.3°

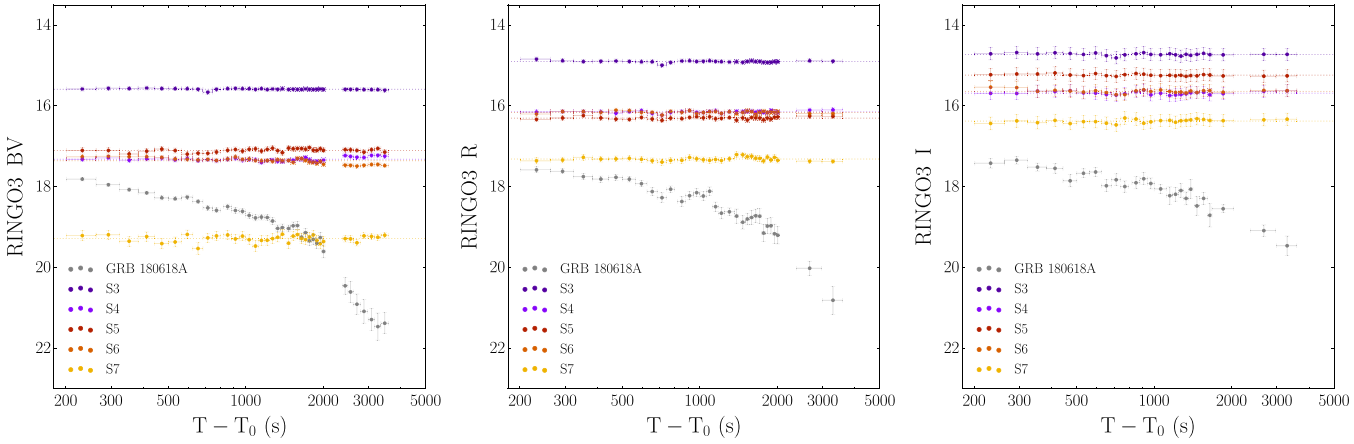

Figure 4. RINGO3 photometric analysis of the field stars (S) in Figure 3 using the temporal binning of the GRB 180618A light curves. Note that stars S1 and S2 are not included in the analysis because the LT repointed to the GRB 180618A coordinates after the IO:O observations, and they fall outside of the revised RINGO3 field of view. From left to right, panels correspond to the RINGO3 *BV*, *R*, and *I* bands.

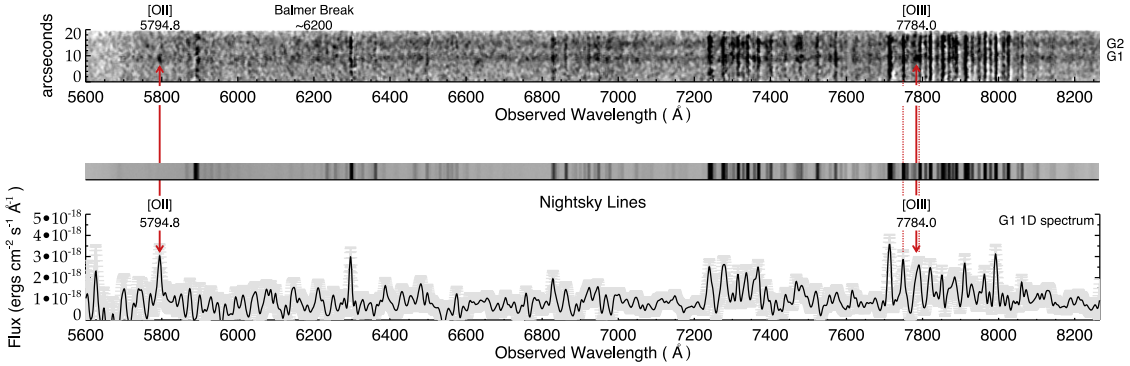

Figure 5. From top to bottom: two-dimensional MODS-2 spectra of the galaxy G2 and the GRB 180618A host galaxy (G1), corresponding night-sky emission lines, and one-dimensional spectrum of the G1 galaxy. In the G1 spectrum, we identify two oxygen emission lines (corresponding to [O II] and [O III]) redshifted at $z = 0.554 \pm 0.001$. The night-sky spectrum displayed here demonstrates that both oxygen emission lines (marked in solid red arrows) are not unsubtracted night-sky emission lines; the [O II] line is not coincident with any night-sky line, and the [O III] line is found between two (dotted red lines).

was used for observations. The position angle was selected so that the target galaxies and the foreground star (≈47″ away) were vertically aligned. The foreground star was aligned in the center of the slit as the target galaxies were too faint to be detected in the acquisition images without incurring too large of an overhead. Two exposures of 20 minutes each were obtained in each channel, with each MODS. The mean airmass of the observations was ≈1.85. The mean seeing (as measured from the off-axis wave front sensor and guiders) was $1.92 \pm 0.''05$ and $1.84 \pm 0.''04$ for MODS-1 and MODS-2, respectively. Observations of the spectrophotometric star BD +33 2642 were used to flux calibrate the data and remove the instrumental signatures from the data.

The MODS data were reduced first with the *modsCCDRed* v2.04 package developed by the MODS team (Pogge 2019) to remove the bias and flat-field the data using a slitless pixel flat. Next, custom IRAF scripts (Tody 1986) were used to extract along the central slit using a stellar trace. The observations of the spectrophotometric standard were combined to measure the trace of the dispersion along the entire slit. This trace was used along with the wavelength calibration from arc-lamp lines to rectify the tilt in both *x* and *y* directions for the full frame (8192 pixels × 3072 pixels). This step made the *x*-axis parallel to the dispersion direction and the *y*-axis purely parallel with the spatial extent along the slit. Final wavelength calibration was cross-checked with known strong auroral skylines in the blue ([O I] $\lambda = 5577.3$ Å) and red ([O I] $\lambda = 6300.3$ Å) channels. One-dimensional spectra were then extracted from each channel using a $1.''85$ wide aperture. This value was chosen to match the mean seeing of the observations, maximizing the signal-to-noise ratio. Next, the spectra were flux-calibrated using the spectrophotometric standard star. Telluric features were removed from the red channels using a normalized spectrophotometric standard spectrum.

Inspection of the data showed no flux from the galaxies in the blue channels of both MODS. A faint but significant continuum was detected for the galaxies in MODS-2 (see Figure 5), but not in MODS-1. The absence of flux in MODS-1 is consistent with a known technical issue[17] in which the sensitivity of the instrument has decreased by a factor of 1.6 since the 2011 commissioning. As a sanity check, the acquisition images were rechecked to confirm no differences in the alignment of the foreground star. The continua of the target galaxies are clearly visible in the individual background-subtracted exposures for the red channel of MODS-2 (see Figure 5). The spatial position (*y* direction) of the continua

[17] https://scienceops.lbto.org/mods/preparing-to-observe/sensitivity/

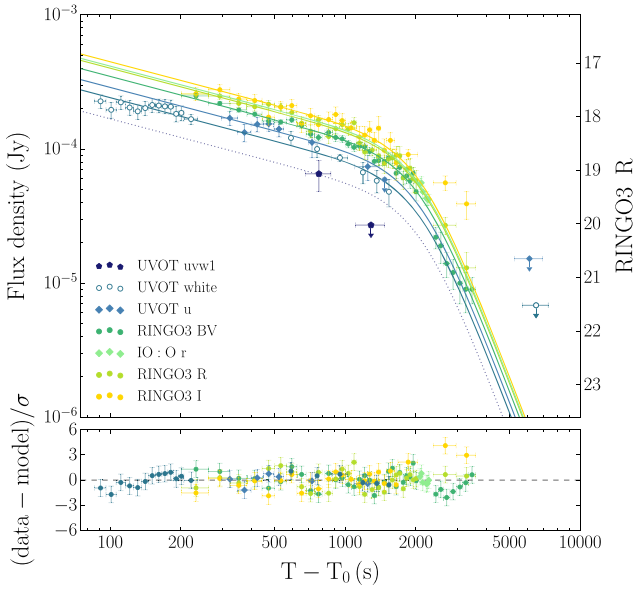

Figure 6. RINGO3 *BV-*, *R-*, *I*-band and UVOT *white-*, *u*-band data modeled with smoothly connected broken power laws that have a common time break across bands. The results of the fit are a break at $t_{\rm break} = 2120 \pm 60$ s post-burst and power-law indexes of $\alpha_1 = 0.46 \pm 0.02$ pre-break and $\alpha_2 = 4.6 \pm 0.3$ post-break with $\chi^2/\,{\rm dof} = 128/116$. We also show with a dotted line the best-fitting model normalized to the near-ultraviolet UVOT *uvw1* band, which has a power-law decay $\alpha_{uvw1} > 1.7$ pre-break. Detections have 1σ error bars, and nondetections are presented as 3σ upper limits.

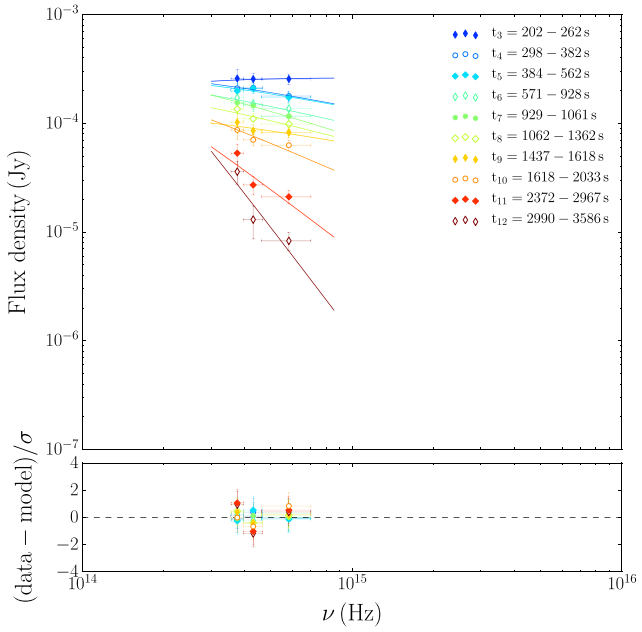

Figure 7. Modeling of the GRB 180618A RINGO3 optical emission with power-law models. Note that the model accounts for Galactic dust extinction but does not include the host galaxy dust contribution.

from the target galaxies detected in the MODS-2 red channel exactly matched the angular separation between them and the foreground alignment star—as measured from the LBC images (see Figure 3). The final calibrated MODS-2 red channel data have a fixed instrumental resolution of 8.19 Å per resolution element covering 5600–10100 Å, which corresponds to a resolution of $R \approx 630$–1350 and 0.84 Å pixel^{-1}. These values were confirmed using the arc lamps.

3. Results

In Section 3.1, we present the temporal and spectral analysis of the optical emission. In Section 3.2, we estimate the redshift of GRB 180618A using the ultraviolet and optical photometry of the transient emission, and we then associate GRB 180618A with its host galaxy. In Sections 3.3–3.5, we study the gamma-ray properties of short GRB 180618A and its extended gamma-ray emission.

3.1. Optical Emission

We simultaneously fitted the UVOT *white*, RINGO3 *BV, R, I*, and IO:O *r* optical light curves with smoothly connected broken power laws (Beuermann et al. 1999; Molinari et al. 2007), i.e., $F = F_0[(t/t_{\rm break})^{n\alpha_1} + (t/t_{\rm break})^{n\alpha_2}]^{-1/n}$, fixing the time break across bands and the smoothness parameter to $n = 1$ for convergence (Piranomonte et al. 2008). This serves to help us understand the overall decay rate of the emission, as well as to check for color evolution in the residuals of the best-fitting model. The emission initially decays with $\alpha_{\rm opt,1} = 0.46 \pm 0.02$ and suffers a sharp break at $t_{\rm break} = 2120 \pm 60$ s post-burst, with $\alpha_{\rm opt,2} = 4.6 \pm 0.3$ (see Figure 6).

This extreme flat-to-steep decay evolution is rare in GRB light curves. To our knowledge, the only other GRB that has shown a similar flat-to-steep decay rate transition ($\alpha_{\rm opt,1} = 0.44^{+0.08}_{-0.21}$ to $\alpha_{\rm opt,2} = 5.3 \pm 0.2$) was found in the fainter optical emission of short GRB 070707 (Piranomonte et al. 2008) and at a much later time, ≈1.8 days post-burst. In addition, in GRB 180618A the spectral evolution across the break is chromatic; the RINGO3 *I*-band emission is significantly underestimated by $>3\sigma$ after the break, and the normalized best-fitting model overestimates the 3σ photometric upper limit of the near-ultraviolet UVOT *uvw1* band. Furthermore, we individually fitted the flux decay rate of the RINGO3 *BV, R, I* and IO:O *r* bands after the break with a power law, finding moderate slopes for redder bands, i.e., $\alpha_{\rm opt,\{BV,r,R,I\}} = 4.6 \pm 0.5,\ 3.5 \pm 0.5,\ 3.2 \pm 0.1,\ 1.4 \pm 0.2$.

Using Xspec v12.9.1 (Arnaud 1996) and χ^2 statistics, we modeled the RINGO3 data with a power law that accounts for Milky Way dust extinction, i.e., $E(B-V)_{\rm MW} = 0.065 \pm 0.003$ (Schlegel et al. 1998). We find that the optical photon index significantly evolves during observations, from $\beta_{\rm opt,PI} = 0.7 \pm 0.4$ at $t = 202$–263 s post-burst to $\beta_{\rm opt,PI} = 4.0 \pm 0.8$ at $t = 2990$–3586 s post-burst; see results in Figure 2 (bottom panel), Figure 7, and Table 2. Note that if we include the UVOT data, we need to add the host galaxy dust extinction to the model, which shifts all optical photon indexes by the same amount toward harder values (i.e., the relative evolution of the $\beta_{\rm opt,PI}$ remains the same).

3.2. Redshift and Host Galaxy

We rule out a high-redshift origin given the detection of the GRB 180618A optical counterpart with all the UVOT filters (Krühler et al. 2011). We used the *uvot2pha* tool to convert the UVOT data to Xspec spectral files, and a dust-absorbed power law that includes both Milky Way and host galaxy contributions, i.e., $E(B-V)_{\rm HG}$. Taking the spectral coverage up to the far-ultraviolet of the UVOT *uvw2* filter into account and using the redshifted Lyman-limit break at $\lambda_{\rm obs} = 912(1+z)$ Å, we fitted the co-temporal UVOT and RINGO3 data corresponding to 550–1600 s post-burst using χ^2 statistics. We estimate a